ORIGINAL PAPER

An experimental study on aging effects of fuel-cut events including sound optimized torque reduction on modern three-way catalysts

René Eickenhorst[1,2] · Thomas Koch[1]

Abstract

Continuously increasing country-specific emission standards for passenger vehicles demand additional development steps in complex exhaust gas aftertreatment systems for a more effective reduction of harmful gases. The efficiency of the aftertreatment system declines over its lifecycle due to specific load profiles and other boundary conditions, resulting in increasing emissions over vehicle mileage. As a result, the durability of the exhaust system becomes more important. Fuel cut is an intended, temporary interruption of the fuel supply of modern combustion engines of passenger cars to reduce fuel consumption and emissions. During this fuel reduction event, unconsumed oxygen of rich and cool fresh air is introduced to the combustion chamber and to the exhaust system. Besides a catalyst cool down, oxidation effects are provoked by enhanced oxygen reactions processes within the catalyst's washcoat and surface layers. In this publication, specific aging cycles with a variation of fuel-cut programs were examined on their effects on a modified modern eight-cylinder turbo-charged engine, especially on their oxidation effects correlating to catalyst aging. Light-off curves and conversion heat maps were used to evaluate possible damaging impacts of fuel-cut events on the aging behavior of the catalyst systems. Results indicate that higher frequency of fuel-cut events results in a reduced catalyst conversion efficiency, whereas thermal sintering might be reduced due to overall lower temperature load. Temporary oxidation processes on catalyst's surfaces occur only in a short timespan after changing the air fuel ratio to lean, resulting in a weaker thermal sintering during longer fuel-cut events. Sound optimized torque reduction functions, used in sports cars for a better drivability and powertrain response, exhibit a stronger aging influence due to additional thermal shock effects on the catalysts front face, as demonstrated via optical infrared sensor technology during catalyst aging cycles on the modified engine bench setup. A theoretical calculation of aging processes as a combination of thermal sintering by Arrhenius equation as well as oxidation process is discussed to describe an aging classification induced via oxidation processes. Additional physisorption measurements of different catalyst probes support the results which indicate the direction of future experimental approaches.

Keywords Catalyst aging/deactivation · Upcoming emissions legislations · Vehicle durability · Fuel cut · Oxidation process · Light-off · Conversion efficiency maps · Sound optimized torque reduction (SOTR) · Exothermic behavior · Arrhenius equation

List of symbols

AFR	Air–fuel ratio
BET	Gas analysis technique after Brunauer, Emmet and Teller for determination of effective surface of materials
BEV	Battery electric vehicle
C-mode	Driving mode "Comfort"
C	Carbon
Ce	Cerium
CO	Carbon monoxide
CO_2	Carbon dioxide
CARB	California Air Resources Board

✉ René Eickenhorst
rene.eickenhorst@mercedes-benz.com

Thomas Koch
thomas.a.koch@kit.edu

1   IFKM (Institut Für Kolbenmaschinen)-KIT, Karlsruhe, Germany

2   Mercedes-AMG GmbH, Affalterbach, Germany

🖄 Springer

|	
cGPF	Coated gasoline particular filter
F_{Oxi}	Oxidation factor
$F_{Arr_{heatloss}}$	Arrhenius heat loss factor
$F_{LO_{change}}$	Light-off change factor
FC	Fuel cut
GPF	Gasoline particular filter
ECU	Engine control unit
EPA	U.S. Environmental Protection Agency
H	Hydrogen
h	Hour
H_2O	Water
HC	Hydrocarbon
HEV	Hybrid electric vehicle
Hz	Hertz
K	Kelvin
km	Kilometer
LEV	Low emissions vehicle
LO	Light-off
m	Mass
$\dot{m}$	Mass flow
mfb_{50}	Center of combustion, at which 50 percent of the fuel mass has been burned off
ms	Millisecond
mi	Miles
MIL	Malfunction indicator lamp
μm	Micrometer
N	Nitrogen
NO_x	Nitrogen oxide
O	Oxygen
Pd	Palladium
PGM	Platinum group metals
PHEV	Plug-in hybrid electric vehicle
Pt	Platinum
QP	Mercury intrusion porosimetry
R	Thermal reactivity constant
R-mode	Driving mode "Race"
Rh	Rhodium
rpm	Rounds per minute
$S_{Arrhenius}$	Summation of aging time over all temperature bin
$S_{Arr_{loadfuelcut}}$	Summation of aging time over all temperature bin for temperatures below $T_{thresh_{Arr}}$
$S_{Arr_{load}}$	Summation of aging time over all temperature bin for temperatures above $T_{thresh_{Arr}}$
S-mode	Driving mode "Sport"
S+-mode	Driving mode "Sport Plus"
SOTR	Sound optimized torque reduction
TWC	Three-way catalyst
T_{50}	Catalyst temperature, whereat 50% conversion ratio has been reached
t_h	Aging time within specific temperature bin T_v
t_e	Overall aging time for each temperature bin
T_r	Reference temperature
$T_{r_{fuelcut}}$	Reference temperature for temperatures below $T_{thresh_{Arr}}$
$T_{r_{load}}$	Reference temperature for temperatures above $T_{thresh_{Arr}}$
$T_{thresh_{Arr}}$	Threshold for Arrhenius separation
T_v	Midpoint temperature of each temperature bin
λ	Lambda

1 Introduction

Indications of climate change effects can be identified in all regions of the world, increasing global demands on environment protection over the last decades, especially within the last years. One approach towards a reduction of CO_2 emissions is stricter legislations for exhaust emissions of automobiles. As a result, manufactures started to electrify their vehicle powertrains a couple of years ago. In addition to battery electric vehicles (BEV), which produce zero gaseous emissions locally, improved conventional combustion engines (ICE) and hybrid powertrains (HEV & PHEV) will also play an important role to fulfill individual mobility demands over the next decades in some regions. Due to this progressing technology change, it is important to optimize the technology of the exhaust aftertreatment system even more to ensure the compliance with governmental requirements. Besides further reduction of threshold values for specific emissions, new emission types will be regulated by upcoming legislation. On top of this, requirements for durability and emission stability of exhaust aftertreatment systems over vehicle lifetime might be extended in future, as well. Current EU6d type V legislation demands service life for exhaust systems of passenger cars up to 160,000 km. The California Air Resources Board (CARB) demands for its LEVIII legislation durability goals of 150,000 miles, corresponding to 243,000 km. One major component within the exhaust aftertreatment of a gasoline engine is the three-way catalyst, whose substrate with its active catalytic washcoat is responsible for the reduction of harmful gases during engine operation. To ensure low emissions over vehicle lifetime, efficiency has to be maximized. The catalyst efficiency decrease is called "aging" and is caused by different factors. One of these factors are oxidation processes, which occur on the catalyst surface during fuel-cut engine mode, induced by the response of the engine controller to driver performance demand. Within this article, the influence of the characteristics of fuel-cut effects on the catalyst durability is analyzed under high engine load conditions regarding different frequencies as well as durations of fuel-cut events. Additionally, the influences of the so-called sound optimized torque reduction (SOTR) functions, employed primarily in

performance orientated vehicles, are analyzed on their influence on exhaust system aging [1, 2].

2 Catalytic deactivation (state of the art)

2.1 Exhaust gas aftertreatment of a gasoline combustion engine

An internal combustion engine converts chemical into mechanical energy, which is used for powering the vehicle powertrain. A modern gasoline combustion engine requires the supply of gasoline fuel as well as air in a precisely controlled ratio. The mixing of both reaction partners into an ignitable mixture within the combustion chamber and its ignition caused by a spark provides momentum to the piston, resulting in a turning movement of crankshaft. For optimal combustion, three fundamental requirements must be fulfilled. The fuel has to be finely dispersed and preferably evaporated and mixed with a sufficient amount of oxygen. The ratio between the mass of air and fuel is determined by the AFR (air–fuel ratio), which must be provided for a complete oxidation of the hydrocarbons of the fuel

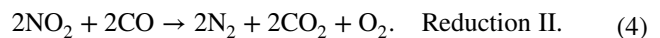$$C_xH_y + \left(x + \frac{1}{4}y\right)O_2 \rightarrow x\,O_2 + \frac{1}{2}yH_2O. \quad \text{Combustion process.}$$
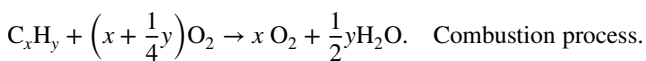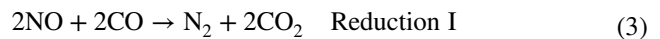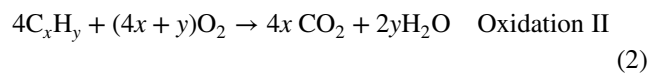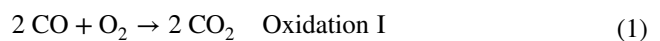
As a result of using fresh air, which consists out of different gases besides oxygen, and technical limitations leading to a partial incomplete combustion, harmful byproducts are part of the exhaust gas of a combustion engine. Most of these harmful emissions are regulated by country-specific governmental legislations. To fulfill these requirements, the most harmful compounds are converted into less toxic substances by catalytic converters downstream of the combustion engine, mainly by a so-called three-way catalyst coating of finely dispersed precious metals on a ceramic substrate, used for parallel oxidation and reduction processes of the exhaust gas species. Figure 1 illustrates a schematic structure of a combustion engine and its emissions' control components.

2.2 Three-way catalyst

As explained in chapter 2.1, the three-way catalyst is one of the main components within the gasoline exhaust gas aftertreatment system, responsible for converting the three harmful gaseous emission groups CO, HC and NO_x into less harmful CO_2 and N_2 via the following oxidation and reduction reactions:

$$2\,CO + O_2 \rightarrow 2\,CO_2 \quad \text{Oxidation I} \tag{1}$$

$$4C_xH_y + (4x + y)O_2 \rightarrow 4x\,CO_2 + 2yH_2O \quad \text{Oxidation II} \tag{2}$$

$$2NO + 2CO \rightarrow N_2 + 2CO_2 \quad \text{Reduction I} \tag{3}$$

$$2NO_2 + 2CO \rightarrow 2N_2 + 2CO_2 + O_2. \quad \text{Reduction II.} \tag{4}$$

During a stoichiometric engine operation, both types of reactions occur at the same time. Oxidative and reductive reactions are exothermic and require a catalyst layer-specific activation energy corresponding to a surface temperature of around 200–300 °C. To ensure a sufficient aftertreatment efficiency during an engine cold start, a three-way catalyst is mostly positioned as close as possible to the exhaust manifold. In modern three-way catalysts, the substrate, usual made out of a ceramic material, is embedded in a metal canning by a damping mat (Fig. 2). The substrate, or so-called
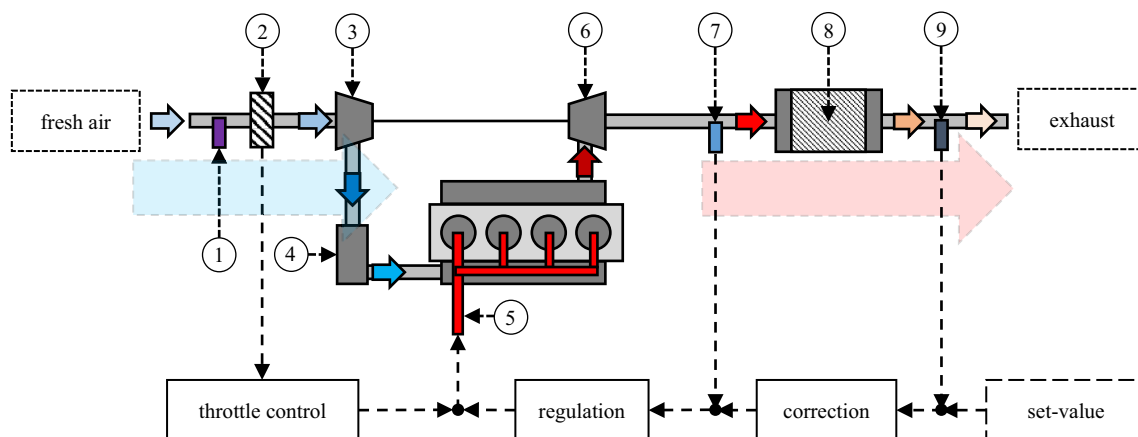

Fig. 1 Simplified diagram of the air–fuel ratio (AFR) control of a turbo-charged four-cylinder engine (according to Riegel, Neumann, and Wiedemann; 1: airflow sensor; 2: throttle; 3: compressor; 4: charge-air intercooler; 5: fuel system; 6: turbocharger; 7 & 9: lambda oxygen sensor; 8: three-way catalyst (TWC) [3, 4]
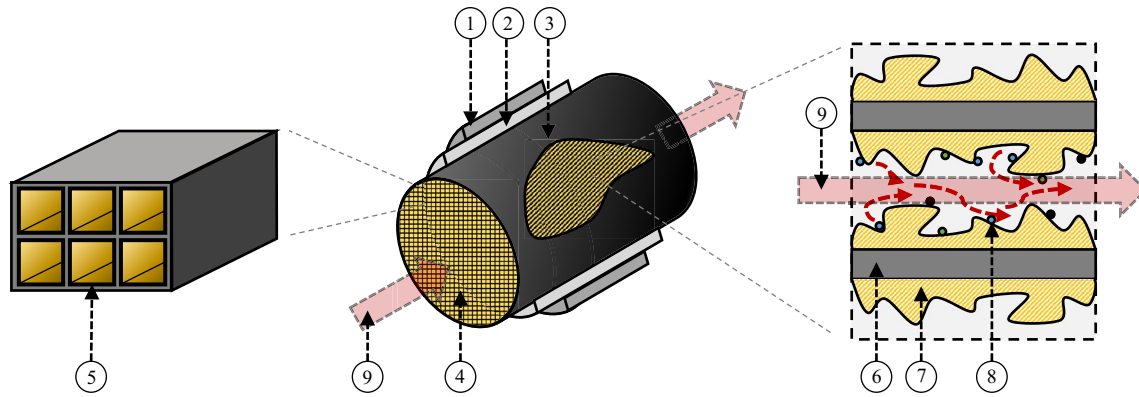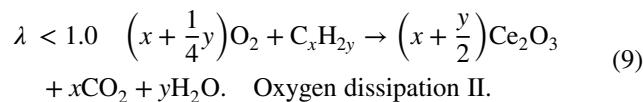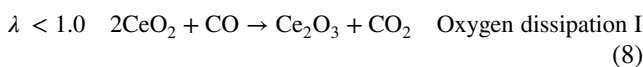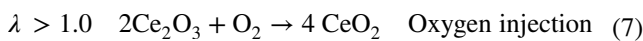
Fig. 2 Schematic setup of a modern ceramic three-way catalyst; 1: canning; 2: damping mat; 3: ceramic monolith; 4: front surface; 5: channels; 6: ceramic wall; 7: washcoat; 8: finely distributed precious metals; 9: exhaust gas flow [21]

monolith, consists in most cases of ceramic with a high thermomechanical stability. Its honeycombed channels, arranged in downstream direction, provide a maximum surface to ensure sufficient conversion ratio even at high exhaust mass flow. This surface is increased by additional application of a washcoat and a top layer, accommodating the fine dispersed precious metal particles of Rhodium (Rh), Palladium (Pd), and Platinum (Pt), responsible for the catalytic effects. To always provide a sufficient amount of oxygen, it can be stored and released via cerium dioxide (CeO_2) embedded in the washcoat

$$\text{stoichiometric AFR} = \frac{m_{\text{air}}}{m_{\text{fuel}}} = 14.7 \quad \text{Air fuel ratio (AFR)} \tag{5}$$

$$\lambda = \frac{\text{current AFR}}{\text{stoichiometric AFR}} = \frac{\frac{m_{\text{air}}}{m_{\text{fuel}}}}{14.7}. \quad \text{Lambda } (\lambda). \tag{6}$$

During lean engine operation with $\lambda > 1.0$, excess oxygen can be stored via oxidation of the ceroxide. In rich exhaust gas conditions ($\lambda < 1.0$), the oxygen stored before by cerium oxides is released to provide oxidative capacities (Eqs. 1, 2) even under these conditions. The ability to store and release oxygen is determined by the oxygen storage capacity (OSC) [4–13]

$$\lambda > 1.0 \quad 2Ce_2O_3 + O_2 \rightarrow 4\,CeO_2 \quad \text{Oxygen injection} \tag{7}$$

$$\lambda < 1.0 \quad 2CeO_2 + CO \rightarrow Ce_2O_3 + CO_2 \quad \text{Oxygen dissipation I} \tag{8}$$

$$\lambda < 1.0 \quad \left(x + \frac{1}{4}y\right)O_2 + C_xH_{2y} \rightarrow \left(x + \frac{y}{2}\right)Ce_2O_3$$
$$+ xCO_2 + yH_2O. \quad \text{Oxygen dissipation II.} \tag{9}$$

2.3 Deactivation processes in modern three-way catalysts

As already stated in the introduction, governmental legislations demand emission stability over a specific vehicle lifetime. As a consequence of loss of effectiveness due to a reduction of the catalytic conversion rate. The emissions levels are allowed to exhibit a distinct increase over vehicle lifetime but have to fulfill country-specific thresholds over required mileages. Three-way catalyst deactivation, also referred to as catalyst aging, can be generally separated into the following four different pathways (Table 1).

Deactivation can be caused by aging processes of the substrate/monolith, of the washcoat applied on the ceramic surface or even of the catalytic centers itself. In most cases, the effective surface of the three-way catalyst is reduced over lifetime, leading to less-active participation in the conversion of exhaust gas components and subsequent higher emissions. Geometrical blocking of the TWC surface, mostly by (hydro-) carbon particles as a result of inhomogeneous combustion, is described as fouling. Carbon residues can be oxidized by oxygen ($\lambda > 1.0$) only at high exhaust temperatures above 500 °C. Deactivation by chemical poisoning reduces the catalytic activity as a result of active elements like sulfur binding to the surface of the catalytic precious metals. Due to improved powertrain components as well as a restriction regarding the sulfur amount within the gasoline fuel, the amount of poisoning deactivation could be strongly reduced during the last decades. Mechanical deactivation describes the degradation due to mechanical surface abrasion and thermal shock events of monoliths. Particles formed during combustion processes or stripped deposits of the engine periphery parts impact the catalyst and result in mechanical damage of the brittle ceramic structure. Additional mechanical degradation might be

Table 1 Main mechanisms of catalyst deactivation

Aging pathway	Deactivation mechanism
Thermal	Precious metal sintering
	Washcoat sintering
	Interaction between precious metal and washcoat
	Metal vitalization
	Precious metal surface change
	Precious metal oxidation
Chemical	Poisoning
	Inhibition
	Reconstruction of the catalytic surface by poisoning element
	Physical/chemical blocking of the pore structure
Mechanical	Thermal shock
	Abrasion
	Loss of stability
Fouling	Deposit of carbon

induced by the so-called thermal shock, caused by extreme temperature gradients on the TWC surface exceeding 15 K/ms. Exhibiting the catalyst surface to a drastic temperature change within a very short time span will result in high internal tensions leading to cracks and subsequent breakdown of surface structures. The largest effect on catalyst deactivation is associated with thermal sintering, a slow, gradual process as a function of time and temperature. The TWC's resistance to this degradation is depending on the washcoat's mix of materials as well as to its precious metal load composition. Higher engine exhaust temperatures lead to a more aggressive catalyst aging. First sintering reactions are described between temperatures of 800–850 °C, whereas maximum exhaust temperature operation points can exceed 1000 °C. This process can be intensified by the presence of oxidative atmosphere. Sintering reactions provoke washcoat collapse or agglomeration of the catalytic precious metals (PGM). In both ways, effective surface is reduced, resulting in higher emissions. Washcoat collapse can be determined via physisorption measurements, and PGM agglomeration can be documented via a chemisorption method [2, 5, 6, 8, 11, 13–18].

2.4 Engine fuel-cut mode and its influence on catalyst deactivation

Fuel cut is an intended, temporary interruption of the fuel supply in phases where no power delivery is requested via the combustion engine. In this case, the engine is towed via the vehicle momentum only. Although air is streaming through the combustion chamber, it is not required to inject fuel, because the engine rotation is sustained via the powertrain. As a result of the friction torque of the drive train, the vehicle speed is constantly reduced.

Normally fuel cut is initiated gently by the engine control unit (ECU). For creating an adequate driving comfort, the amount of injected fuel is ramped out smoothly and engine power output is decreased over a couple of combustion cycles. In addition to this, the ignition timing and the center of combustion (mfb_{50}) is set to late, creating less power output with a low engine efficiency factor.

In performance orientated cars, a different fuel-cut characteristic is employed. To provide a reproducible and direct drivability, fuel cut is induced more directly and abrupt, resulting in less comfort and a rougher powertrain beating. The abrupt torque reduction is implemented via a large change of the ignition angle to late as well as consequent cylinder fade-outs. By setting up a late ignition timing in combination with a late exhaust valve closing, part of the combustion is taking part within the exhaust manifold. Usually, this results in an overlay of the acoustic waves within the exhaust system itself, noticeable from the inside and outside of the passenger vehicle. These acoustic phenomena can be optimized via the engine control unit by changing the timing based on torque request, engine speed, and other different factors, known as sound optimized torque reduction (SOTR).

In case of a fuel-cut event, only fresh air streams through the three-way catalyst ($\lambda = \infty$). By this, oxidation processes (Eqs. 1, 2) and oxygen storage (formula 7) are taking place on the three-way catalyst's surface. As explained in chapter 2.2, oxidative processes are exothermic reaction, which means that in case of a fuel cut, exhaust temperatures are increased as long as the oxidative reactions occur. Based on the amount of remaining Hydrocarbons HC on the catalyst surface, product of an AFR-swing or a prior rich combustion, the oxidation can have different characteristics, resulting in an extended or

higher exhaust temperature plateau. This increased temperature level results in stronger catalyst aging [19].

Oxygen storage and the following release processes, in case the fuel-cut mode has been stopped, change the molecular structure and so the volume of the Cerium oxide compounds (Ce(III) to Ce(IV)). This volume change introduces thermal and mechanical stress within the washcoat. In addition to this, active SOTR function, where part of combustion takes place in the exhaust manifold besides cylinder cut offs, creating gas pulse effects including heat waves running downstream and reaching the catalyst substrate on the front face, going along with hearable "crackling" sound and additional exothermal reactions. Besides the higher temperature plateau on the catalyst front face, fading out over the catalyst length, the catalyst aging is intensified via a possible thermal shock induced on the TWC front face, as explained in chapter 2.3. Figure 3 illustrates the temperature profile as well as the effect of the thermal shock via high-temperature gradient on the catalyst front face due to fuel-cut events with active SOTR function [17].

# 3 Experimental methods

3.1 Experimental setup

The following chapter explains the experimental setup. It describes the engine test bench and its modification used for realizing the catalyst aging process, the catalytic exhaust system as well as the integrated sensor system for measuring the AFR and the temperatures, occurrence of thermal shock events, and lambda. Furthermore, the design of experiment as well as its evaluation regarding the identification of the influence of the fuel-cut versus thermal aging on the three-way catalyst are provided.

3.1.1 Catalytic exhaust system and its sensor systems for synthetic aging including SOTR function

An exhaust aftertreatment system of the current transverse four-cylinder engine of Mercedes-AMG has been chosen for this study, which has been used in the prior investigations regarding the AFR-swing influence on the three-way catalyst aging. As already presented in the prior publication, the catalyst layout and layer technology of this exhaust system are state of the art. The one-bank system contains two substrates: an upstream three-way catalyst combined with a coated gasoline particular filter (cGPF) downstream. The main function of the cGPF is to reduce particles within the exhaust gas by a mechanical filtration. Due to its additional catalytic coating, the coated gasoline particular filter supports the chemical conversion of harmful gases, especially during high load engine operations. Both substrates provide an overall catalytic volume of 3.701 L with the TWC contributing a volume of 1.558 L [21].

The synthetic aging process on the engine test bench was controlled via different types of sensors. Due to high exhaust temperatures close to 1000 °C, type K thermocouples have been chosen to control the temperature during the catalyst aging experiment. They were arranged up- and downstream the TWC as well as downstream the cGPF. To identify sensor inertia, sensors with variable diameters were used. Different characteristics of fuel-cut events were part of the experiment, including fuel-cut modes with SOTR function. As explained in chapter 2.3, a thermal shock is defined as temperature change in a very short time, which a thermocouple might not be able to resolve. Therefore, an optical sensor with a sampling frequency of 10 kHz was installed upstream the TWC facing on its front face, enabling the observation and recording of a possible thermal shock. The infrared sensor had already been calibrated prior with the help of a 0.5 mm thermocouple touching the front face of the TWC (Fig. 4) during a slow cool down phase with a sensor correlation over 95%. Oxygen sensors, installed up- and downstream of the TWC, were utilized to regulate the AFR

Fig. 3 Temperature effects on TWC front face due to fuel-cut events with active SOTR function
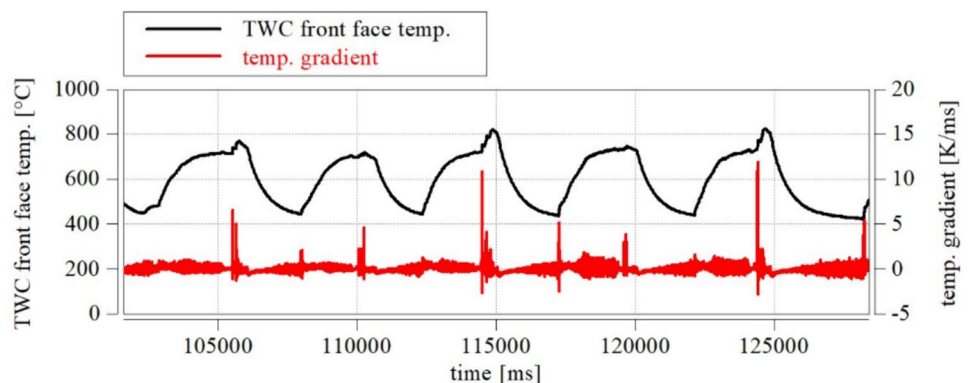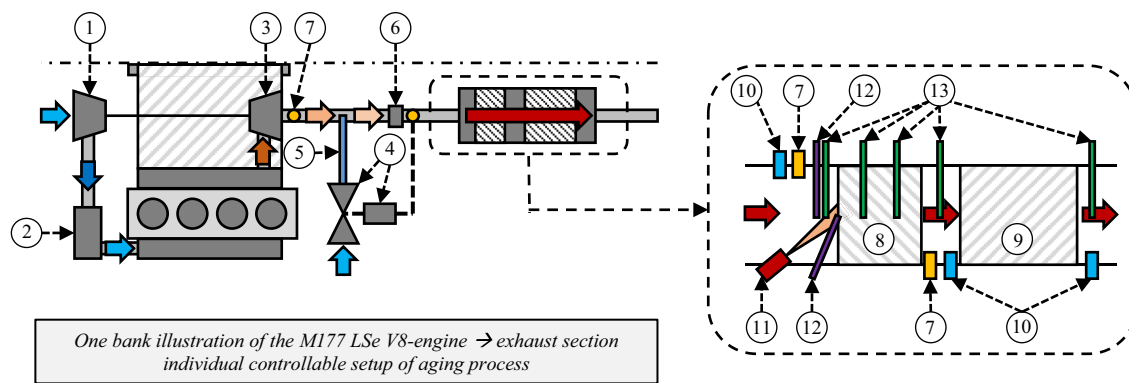
Fig. 4 Modification of an turbo-charged V8 engine (one-bank illustration) and its exhaust aftertreatment system; 1: compressor; 2: charged air cooler; 3: turbo charger; 4: secondary air regulation system and valve; 5: secondary air injection; 6: mixer; 7: oxygen sensor; 8: TWC; 9: cGPF; 10: gas sample point; 11: optical sensor; 12: 0.5 mm thermocouple; 13: 1.5 mm thermocouple [21]

and to detect OSC level changes. To calculate the conversion ratio of the overall aftertreatment exhaust system and so its performance after the synthetic aging process, sampling points for raw gas were set up in front of the TWC and cGPF for measurement of harmful gases like CO, NOx, and HC -emission (Fig. 4—right side) [17].

3.1.2 Modification of a turbo-charged engine for catalyst aging on an engine test bench

As explained within chapter 1, governmental legislation demands emissions stability over vehicle life time, at least up to 160,000 km for EURO 6e. Therefore, it is mandatory to reduce the catalyst aging to a possible minimum by optimizing the catalyst's washcoat, substrate, and layer as well as the engine exhaust aftertreatment calibration. During limited vehicle development phases, even extended vehicle durability runs with a customer-specific load profile cannot provide all information on catalyst ageing behavior. As a result, synthetic catalyst aging on an engine test bench is applied additionally. Compared to durability runs, these tests are more cost-efficient, take less time due to well-controlled engine operation parameters with an increase repeatability and results more comparable to catalysts aged via vehicle mileage accumulation [6, 8, 20].

Engine catalyst aging is usually performed on a natural aspirated engine, which allows exhaust gas temperatures above 950 °C direct behind the exhaust manifold without exceeding components' thermomechanical limits. For the present experimental analysis, a comparable test bench setup has been chosen, which was used during prior AFR-swing studies. This setup has the advantage to provide high exhaust temperatures above 950 °C over a long aging time without a possible thermomechanical defect of the turbocharging component. Sufficient exhaust mass flow can be controlled while employing an overall fuel- and consequently cost-efficient

engine catalyst aging operation. On top of this, the ECU of this state-of-the-art turbo-charged V8 engine has already implemented the functionality of the SOTR function allowing to include the analysis of its possible influence on the catalyst aging in this study.

To compensate the enthalpy losses due to the turbo-charger components to reach high catalyst temperatures, the temperature level behind the outlet valve (T3 temperature) needs to be elevated, exceeding the given temperature durability limit of the turbocharger components. In this case, modifications had to be included to prevent failure of components during long catalyst aging processes. The engine operation was changed to a rich combustion ($\lambda < 1.0$) and a secondary air injection was implemented downstream of the turbocharger. By this, high exhaust temperatures on the catalyst surface can be achieved by creating a catalytic supported exothermic reaction of HC and O_2. The catalysts λ-ratio was controlled directly via the engine lambda, or via adjustment of the secondary air flow. To ensure a stable catalyst AFR, an additional mixer had been integrated into the exhaust path, upstream the TWC front face. Prior studies have shown that this exhaust section individual controllable setup works stable and efficient even over long aging processes above 500 h. Figure 4 illustrates the engine test bench setup with its modification on the M177 LSe V8 engine (left bank) [6, 21].

3.2 Design of experiment

3.2.1 Experimental procedure

The initiation of fuel cut during normal engine operation has already been explained in chapter 2.4. To mitigate possible influence factors during this experimental analysis, a constant engine operation point was kept; meanwhile, fuel-cut events were integrated in regular distance with different characteristics. As explained in chapter 3.1.2, the required

Table 2 Experimental matrix of fuel-cut (FC) study

test	exhaust system ID	Aging				Evaluation			
		FC interval [s]	FC duration [s]	duration [h]	SOTR-function	FC interval	FC duration	aging duration	SOTR function
#1	#A	constant	-	50 & 100	-	✓		✓	
#2	#B	60	5	50	-		✓		
#3	#C	120	3	50	-	✓			
#4	#D	60	3	50	-	✓	✓		✓
#5	#E	30	3	50 & 100	-	✓		✓	
#6	#F	60	3	50	yes				✓

high exhaust temperatures for catalyst aging were generated by creating an exothermic reaction on the catalyst surface by the PGM's via rich exhaust and fresh secondary air, while having a three-way catalyst lambda of 1. To initiate the fuel cut, fuel supply was stopped, and secondary air injection was also shut down to prohibit an unnatural TWC cool down by the fresh secondary air. At the same time, the throttle angle was increased for balancing the overall catalyst exhaust mass flow during the fuel-cut event remaining on the same level as during the combustion operation mode. In some experiments, the SOTR function was activated by changing the drive mode within the ECU. When setting the mode from Comfort (C-mode) to Sport Plus (S + -mode) or even to Race (R-mode), the ECU induced the fuel-cut events with SOTR characteristics. For an active fuel cut and for active SOTR functionality, a special bit is set, which allowed simple identification of these modes during the catalyst aging runs as well as during the analyses of the recorded data (Fig. 6).

3.2.2 Fuel-cut event variation

During this study, four different fuel-cut parameters were analyzed: frequency of occurrence and length of the fuel-cut event were proved to have major influence on the catalyst aging. Due to this, analysis of vehicle durability data has been prioritized to estimate statistic data for these two. As explained in chapter 3.1.1, the exhaust aftertreatment systems aged within this study contained a cGPF and was developed mainly for the European market. Germany, with its open-speed limit highways, represents one of the worst load profiles regarding catalyst aging, so that these country-specific durability runs with this type of engine (M139q) were previously used for an estimation regarding the fuel-cut length and frequency of occurrence. According to references, listed in chapter 2.3, thermal catalyst aging effects first occur around an exhaust temperature of around 850 °C. As a result, vehicle endurance run data from Germany have been analyzed regarding the fuel-cut events at exhaust
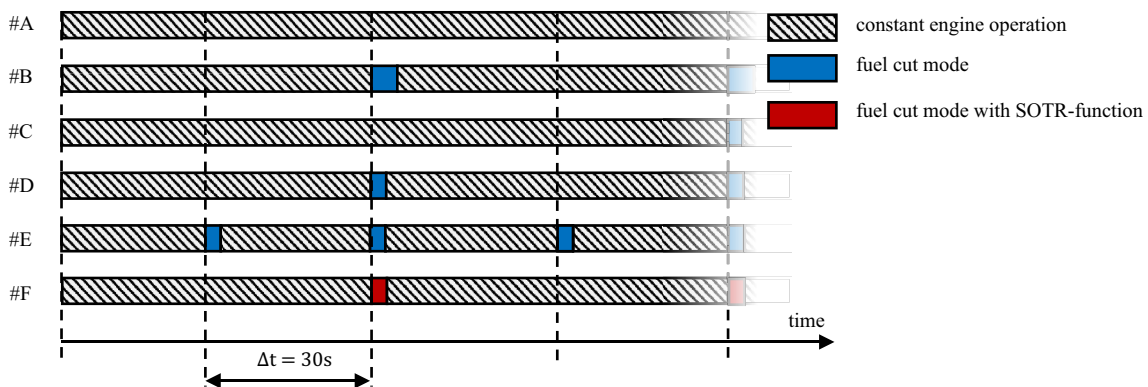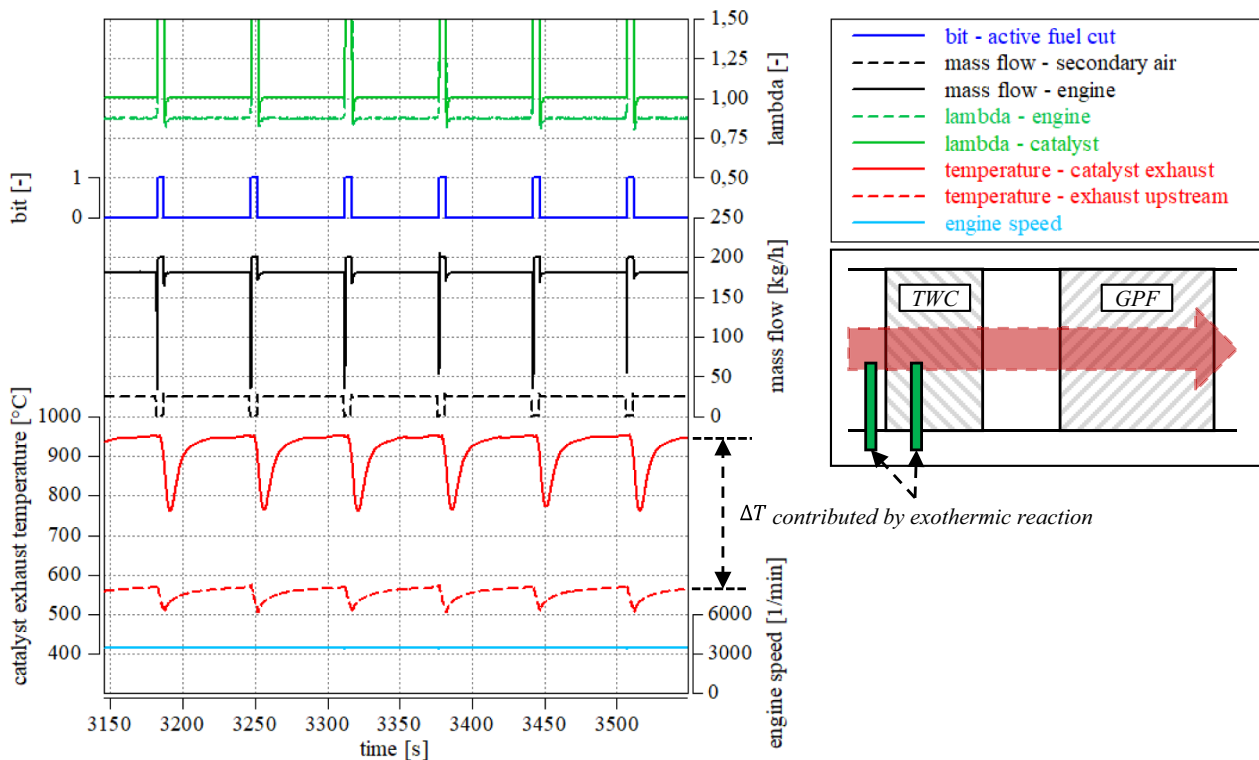

Fig. 5 Fuel cut event variation

Fig. 6 Engine parameters during the aging process of exhaust system #D

temperatures above this specific temperature level. Ninety-five percent of the normal distribution for the fuel-cut length varied between 3 (#D) and 5 (#B) seconds, whereas for the time span between these fuel-cut events, values between 30 (#E) and 120 (#C) s could be obtained. Center of this distribution was located around 60 s, which was set as the initial point for this study (#D). In addition to this, one exhaust system was constantly aged without any fuel cut as kind of a reference for thermal aging without oxidation influences (#A). In another experiment, one catalyst system was aged with an active SOTR function (#F) while using the same aging and fuel-cut boundary conditions as the initial aging sequence (#D). Figure 5 illustrates an overview over the six exhaust systems and aging event variation.

The overall aging duration was set as in prior studies up to 50 h, with two exhaust systems being aged for additional 50 h after first evaluation. Previous analysis has shown that modern state-of-the-art exhaust systems are aging slowly, resulting in a suggestion to enlarge the aging duration for more distinct results. In this study, the exhaust aftertreatment systems with the lowest and highest amount of fuel-cut events are going to be used (#A & #E) to verify this approach of longer test durations. Table 2 illustrates an overview regarding the experimental matrix.

3.2.3 Boundary conditions of the aging procedures

As within prior studies, production deviations based on manufacturing and coating process of layer have shown different light-off and oxygen storage capacity behavior at new condition. Therefore, a short pre-sintering process of all exhaust systems on the engine test bench was conducted at low aging temperatures of around 850 °C for 3 h to guarantee an agglomeration and embedding of the fine dispersed catalytic precious metals, resulting in a comparable light-off and OSC performance [21].

Providing constant boundary aging conditions during this study is essential for an identification of possible fuel-cut influences on the catalyst aging. Therefore, the aging temperature within all catalysts was set to the expected maximum of 950 °C without exceeding thermal boundary conditions. This reduces bench aging time and maximizes the aging effects. The temperatures were monitored via the 1.5 mm thermocouples. Due to the high thermal inertia of the second temperature sensor within the catalyst, the sensor positioned at 1/3 length downstream the TWC front face was used to regulate the aging process. The sensor's failure tolerance at temperatures of around 950 °C was stated as ± 3.8 K, which corresponds to only less than 0.5% of the absolute value. The overall exhaust mass flow within the catalyst has been defined

as the sum of engine exhaust flow and the secondary air injection mass flow. The average exhaust mass flow measured during vehicle durability runs with this modern four-cylinder engine at catalyst exhaust temperatures above 850 °C, is listed at around 200 kg/h. To ensure this constant flow rate during the complete aging processes, the engine speed had been set to a constant value of 3200 rounds per minute (rpm) during fuel-cut events. As explained in 0, the secondary air injection was turned off during fuel cut, while a throttle angle change ensured the constant overall mass flow. The catalyst lambda was set to 1.0 during active engine operation [22].

Figure 6 illustrates the main aging parameters and their effect on measured temperature data on basis of the aging process of catalyst #D. Attention should be paid to the difference of the temperature level between the sensor upstream the TWC and sensor, positioned 1/3 length downstream the TWC front face within the catalyst. This increase of around 300–400 K is contributed by exothermic reaction resulting from the catalytic activity on the catalyst surface.

3.3 Determination of catalyst aging grade via oxygen storage capacity (OSC)

Legislative authority demands a health monitoring of the exhaust aftertreatment system. In case the system has been aged too intensively or was damaged mechanically so that emission standards are no more fulfilled, the malfunction indicator lamp (MIL) has to be set active within the driver's instrument cluster. Different ways for the detection of an inoperative catalyst system have been developed in the past. Besides active sensors, measuring harmful gases directly downstream the TWC, the determination of oxygen storage capacity has been proved to be a robust and effective tool. As shown in chapter 2.2, three-way catalysts use the ability to store and release oxygen through their washcoat to sustain oxidizing environment in rich phases and to allow reductive processes under lean conditions. As explained in chapter 2.3, aging processes
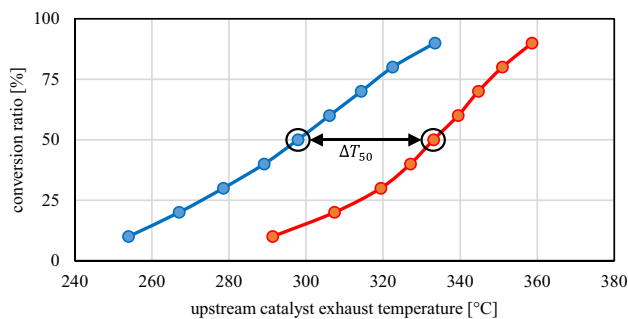
reduce the specific catalytic surface as well as the overall surface of the washcoat responsible for the OSC, so that degradation of oxygen storage capacity corresponds to the regression of the catalytic activity. The OSC is calculated by the ECU during normal driving conditions as follows:

$$m_{O_2} = \int_{t_0}^{t_1} 0,23\left(\lambda_{\text{engine}}(t) - 1\right)\dot{m}_{\text{air}}(t)\mathrm{d}t. \quad \text{Oxygen storage capacity.}$$

(10)

m_{O_2} defines the oxygen storage capacity, and t_0 and t_1 correspond to the duration of the triggered lean to rich switches as recognized by the oxygen sensor in upstream and downstream of the first catalyst. The maximum amount of oxygen, which can be stored within the catalyst, depends on a variation of influence factors (e.g., size of TWC, washcoat, layer) and cannot be generalized [4–6, 8, 11, 23, 24].

3.4 Determination of catalyst aging grade via light-off behavior

The catalytic activity for each gaseous emission can be described as a function of conversion rate of raw gas emissions over the catalyst exhaust temperature. Raw and tailpipe emission probes (Fig. 4—right side) are used to determine the so-called light-off (LO) curve as their quotient plotted over the catalyst exhaust temperature. The T_{50} temperature, defined as catalyst temperature at which 50% of raw gas emissions are converted, is used to characterize the performance of an exhaust system.

Fine and evenly distributed precious metal particles start to agglomerate during thermal sintering by both atomic and crystalline migration processes, resulting in an increase of single particle volume and a drastic reduction of overall active catalytic surface area. Due to this, more energy has to be provided to reach the same activity of the active material as before, resulting in an increase of the T_{50} temperature (Fig. 7). Besides this, the heat release via exothermic reaction is also reduced, why, within this study, the temperature signal via the 1.5 mm thermocouple probe upstream is going to be used to determine the light-off curves without the influence of the exothermal change [6, 8, 19, 25, 26].

3.5 Conversion heat maps for identification TWC performance differences

The catalytic activity for each gaseous emission of an exhaust aftertreatment system can be determined via the light-off behavior as a function of conversion rate over catalyst temperature. Before temperature increases by heat release of exothermic activities within the catalyst, the TWC temperature is also controlled by exhaust mass flow.
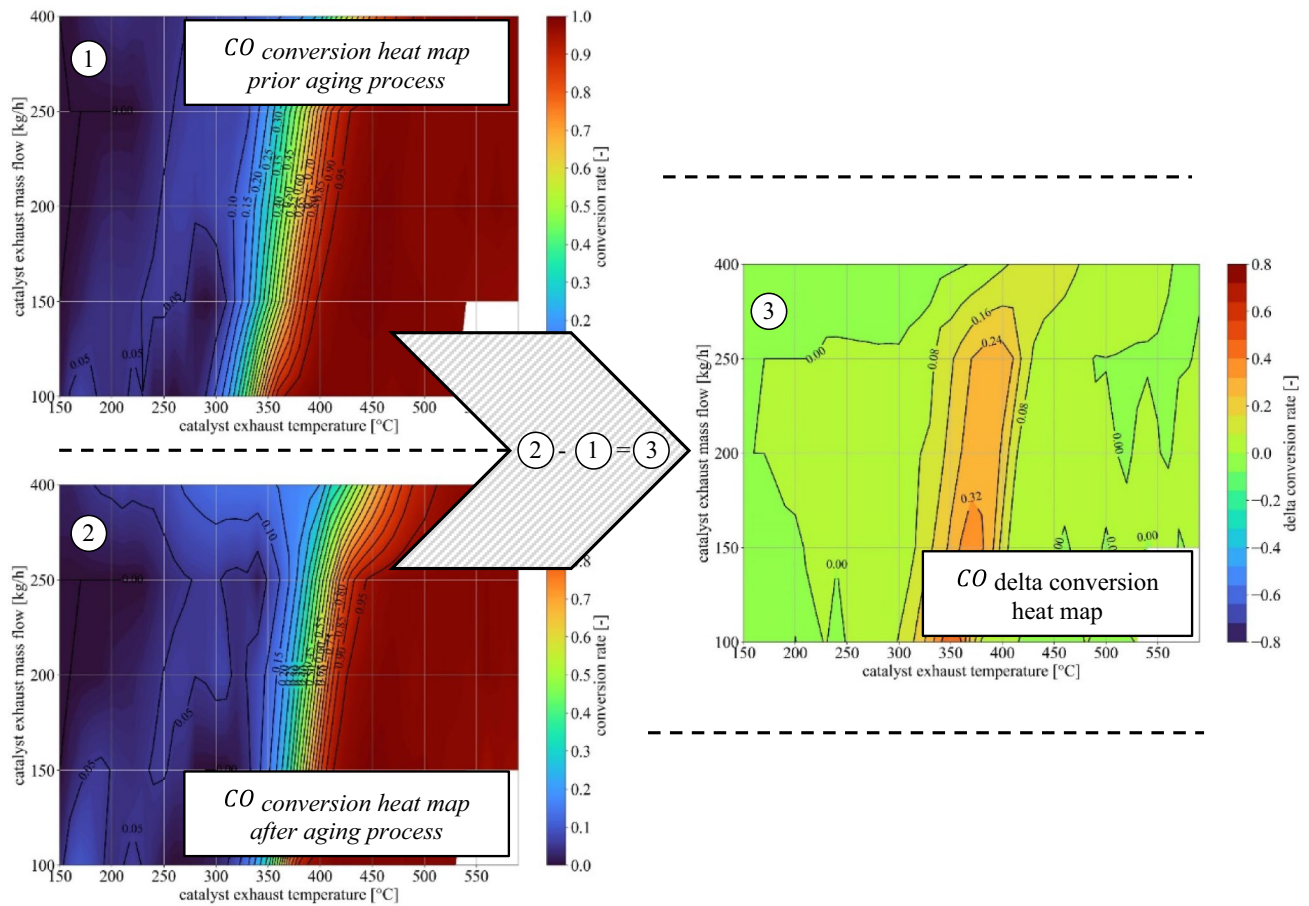

Fig. 7 CO light-off behavior as an example of exhaust system #F before (left) and after (right) aging process

Fig. 8 CO conversion heat map (left) and delta conversion heat map for identification small performance differences (right)

As a consequence of a variable exhaust mass flow during cold starts, provoked by driver-specific load requirements, exhaust temperature is typically transient. To consider this dependency, conversion heat maps are used within this study to determine performance differences of exhaust systems due to catalyst aging, depending on exhaust mass flow as well as catalyst exhaust temperature.

The conversion rates of raw gas emission components were determined on an engine test bench at different constant engine operation points, defined via various exhaust mass flow. Five engine operation points were defined with an exhaust mass flow representing the usual operating map of a passenger vehicle's catalyst. At each constant operation mode, the light-off curve was recorded after a complete cool down to ambient air temperature using a fuel-cut overrun. By this, the washcoat was also enriched with oxygen, so that comparable initial start conditions were ensured. To increase the quality and decrease the scatter of the measured values, measurements for each engine operation were repeated at least three times. These recorded catalytic-specific light-off data served as a basis for interpolating a heat map diagram to display the conversion rate over the regulated exhaust mass flow and rising catalyst temperature (Fig. 8—left side).

Fig. 9 OSC prior and after aging process of exhaust system #D
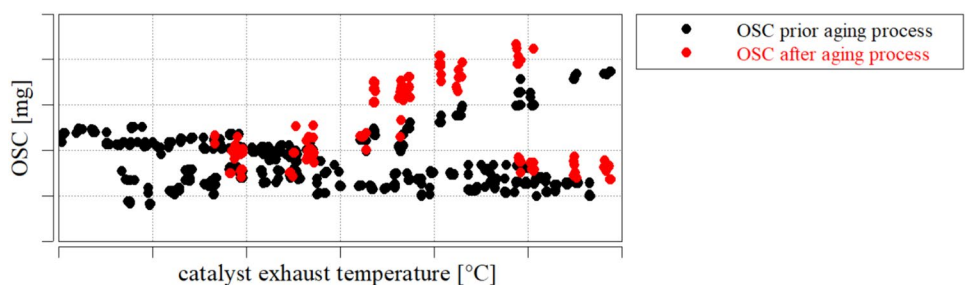
As in prior experimental studies, delta conversion heat maps proved to display the performance differences by aging intensity of different catalysts. Areas with significant performance differences depending on exhaust temperature and mass flow can be easily identified. Figure 8 (right side) illustrates a delta conversion heat map of two differently aged exhaust systems, depending on upstream catalyst exhaust temperature as well as an exhaust mass flow between 100 and 500 kg/h [21].

4 Results and discussion

4.1 Influence of fuel-cut events on oxygen storage capacity

As prior studies have already shown, the triggered lean to rich switches for determination of OSC of this type of three-way catalyst exhibited show small reductions of OSC capabilities for a 50 h aging period. These minimal decreases are shown in Fig. 9: OSC prior and after aging process of exhaust system #D did not allow for a differentiation regarding the aging intensity based on different fuel-cut variations, so that the main focus of further analysis was laid on the specific light-off behavior and the appropriated conversion heat maps.

4.2 Influence of fuel-cut events on catalyst light-off behavior

4.2.1 Fuel-cut frequency (#A—#C—#D—#E)

The effect of the fuel-cut frequency on catalyst aging was analyzed by comparison of the exhaust systems listed in Table 2. The delta conversion ratios, induced by the specific aging processes, are illustrated in Fig. 10 for each exhaust
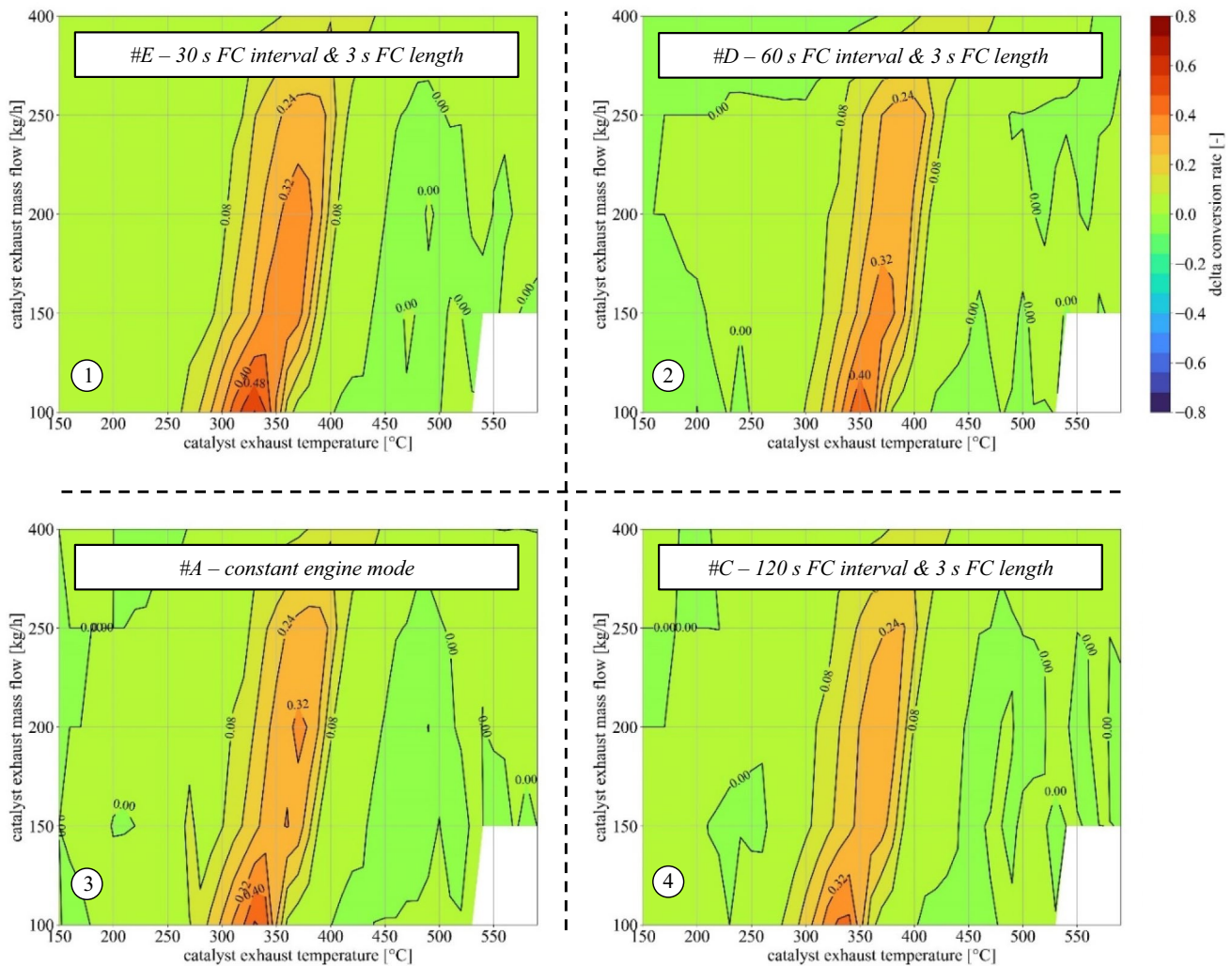

Fig. 10 Interpolated CO delta conversion loss heat map of exhaust systems with different fuel-cut frequencies: 1: #E, 2: #D, 3: #A, 4: #C

system as individual CO delta conversion loss heat maps: the stronger the aging, the more positive the delta value. The delta heat maps for the emission components HC and NO$_x$ depict a comparable behavior.

Aging effects are clearly visible via a decrease of conversion ratio between 300 and 350 °C as well as 100 and 250 kg/h exhaust mass flow. On closer inspection, exhaust system #E with the highest amount of fuel-cut event used within this study shows the strongest aging effect. By reducing the amount of fuel-cut events by about 50% (#D), the aging effect decreases, whereas it is still higher than the aging with constant engine operation mode (#A). The lowest aging effect seems to have the exhaust system #C with fuel-cut events every 120 s.

Increasing number of fuel-cut events exhibit to have a negative impact on catalyst aging, even with the overall heat input for a possible thermal sintering being reduced with higher numbers of events and therefore reduced effect of oxidation as well as the thermal sintering during fuel cuts. With reduced fuel cuts, the effect of oxidation can be neglected, so that the thermal sintering represents the main aging mechanism. The maximum of aging in this study was observed from high thermal loads triggering sintering and oxidation in addition with exothermal reactions during seldom fuel-cut events.

4.2.2 Effect of fuel-cut duration (#D vs. #B)

Oxidizing effects including exothermal reaction with small temperature increases can only be observed for a small timespan due to the limited amount of residual HC on the catalyst surface. Therefore, fuel-cut events of this type of exhaust system with a duration over 3 s do not exhibit any further increase of aging effect. During prolonged fuel-cut events, the cool down of the exhaust system seems to
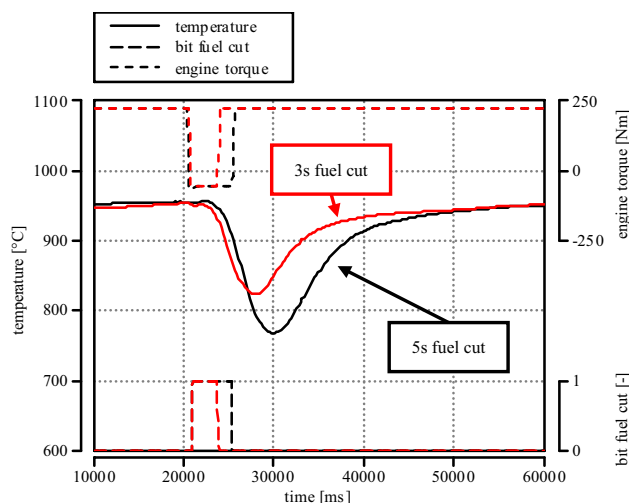
Fig. 12 Effect of fuel-cut duration on catalyst cool down, measured with type K thermocouples within the catalyst

result in a reduced thermal sintering and so less-intense catalyst aging. The effect of cool down, therefore, seems to be more dominant than the effect of oxidation. Figure 11 displays the increased aging of fuel-cut events of 3 s (#D) vs. 5 s (#B) while having the same fuel-cut interval timing. Figure 12 demonstrates the increased cooling effect by extended fuel cut from 3 to 5 s.

4.2.3 Effect of SOTR function (#D vs. #F)

To evaluate the influence of a stricter inset of the fuel-cut effects by activation of the SOTR function, the conversion heat maps of a 3 s fuel-cut duration every 60 s with and without SOTR-parameters were compared. Activated
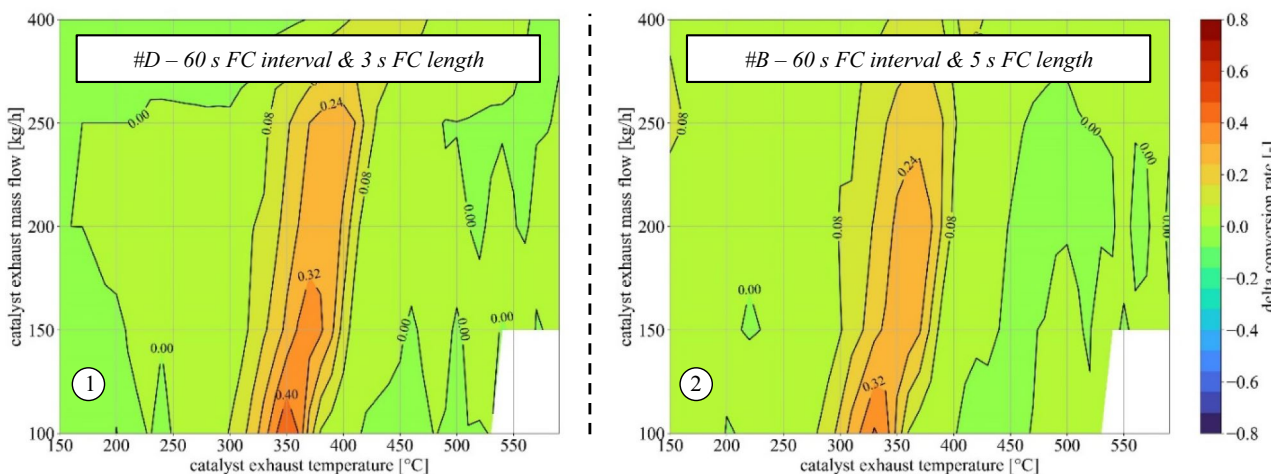
Fig. 11 CO aging effects through different length of fuel-cut events
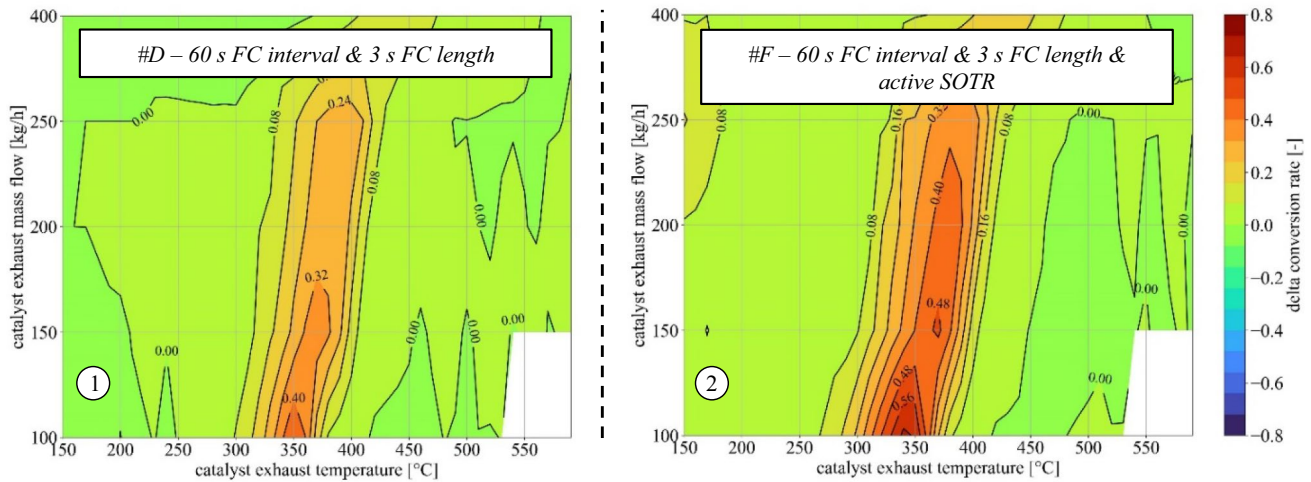
Fig. 13 CO aging effects of 60 s engine operation with 3 s fuel-cut duration without (left) and with activated SOTR function (right)

SOTR function exhibits not only a stronger aging vs. a none-activated aging process but displays also the strongest aging of all exhaust systems in this study. A possible explanation for these intense aging effects could be additional intense thermal shock events leading to catalyst surface degradation, which will be discussed in chapter 4.4 with the help of the optical sensor data, installed upstream of the first three-way catalyst (Fig. 4—right side). Figure 13 illustrates the extended aging effect of the SOTR function (#D vs. #F).

4.2.4 Expansion of aging duration to receive more precise results (#A and #E—50 h vs. 100 h)

As listed in Table 2, two exhaust systems have been additionally aged up to 100 h after first inspection at 50-h test bench run to investigate possible long-term influences of the fuel-cut events. Analysis of the systems after 100 h via delta conversion heat maps showed increased aging but no significant differences regarding overall results. Extended degradation due to a longer aging process was visible; however, the trends observed at 50 h and their distinct patterns remain comparable. From this point of view, 50 h are sufficient to compare the individual parameter effects and can be set for future studies.

4.3 Definition of a characteristic factor for oxidative catalyst aging

Synthetic aging of exhaust systems with a variety of fuel-cut events has been presented in this study. The overall aging has been identified with the help of delta conversion heat maps, based on light-off curves for different exhaust mass flows. Maintaining constant boundary conditions except

the fuel-cut event variation during the aging processes, the overall aging could be described mainly as the summation of oxidation events and damages due to thermal sintering. A mathematical approach to define a characteristic factor regarding the catalyst aging through oxidation will be presented within the following chapters.

4.3.1 Estimation of thermal aging effects by Arrhenius equation

Catalyst aging in form of thermal sintering can be described with the help of the Arrhenius equation as a known method for calculating the aging times corresponding to an exhaust temperature profile. The Arrhenius equation defines the catalyst's thermal load on an engine test bench based on catalyst temperature during vehicle operation. This method allows to obtain comparable catalyst thermal aging on an engine test bench setups in shorter time frames using elevated exhaust temperatures in comparison to a vehicle catalyst driven over a long time or distance. This approach has been proven in the past, so that it found legislative application by EPA and European regulators. The key of this method is that more distinct temperature gradients over a short time exhibit stronger sintering effects than lower temperature slopes over a long time [20, 21, 27–29]

$$\text{Arrhenius}_{\text{factor}} = e^{\left[R\left(\frac{1}{T_\text{r}} - \frac{1}{T_\text{v}}\right)\right]} \quad \text{Arrhenius equation} \quad (11)$$

$$T_\text{r} = \frac{\int_0^{t_\text{end}} T_{\text{AgingCycle}}(t)\text{d}t}{t_\text{end}} \quad \text{Effective reference temperature} \quad (12)$$

$$t_e = t_h * \text{Arrhenius}_{\text{factor}} \qquad (13)$$

Equivalent aging time in each temperature - bin

$$S_{\text{Arrhenius}} = \sum t_e \qquad (14)$$

Summation of aging time over all temperature bin.

T_r describes the arithmetical mean temperature of the aging process and is called effective reference temperature. T_v is the mid-point temperature of each temperature bin, in this study with a width of two Kelvin. R defines the thermal reactivity constant, which has been defined as a value of 17,500, according to the LEV III legislation. t_h stands for the aging time within the specific temperature bin T_v. The overall required aging time is defined as the summation of t_e for each temperature bin, the product of t_h and the Arrhenius$_{\text{factor}}$.

4.3.2 Adaption of Arrhenius equation to fuel cut and engine load operation mode

During fuel-cut events, the temperature of the exhaust and so of the catalyst decreases due to the contact with fresh air. Under consideration of the experimental aging boundary conditions, the temperature, therefore, needs to be separated into different levels. For each level, a specific Arrhenius reference temperature T_r for the duration of engine load and fuel-cut mode is set up to calculate the thermal aging effects. Due to a delayed response of catalyst temperature after activation and deactivation of the fuel cut, the threshold for the separation is defined via the surface temperature change itself and not by the change of engine mode. Within this study, $T_{\text{thresh}_{\text{Arr}}}$ is introduced as a variable, defining the threshold between fuel cut and engine operation mode. It is defined as 99.5% of the temperature used for the aging process itself. Due to this physical, two different synthetic aging durations via the Arrhenius equation can be set up, whereat the overall synthetic aging time is defined by their summation

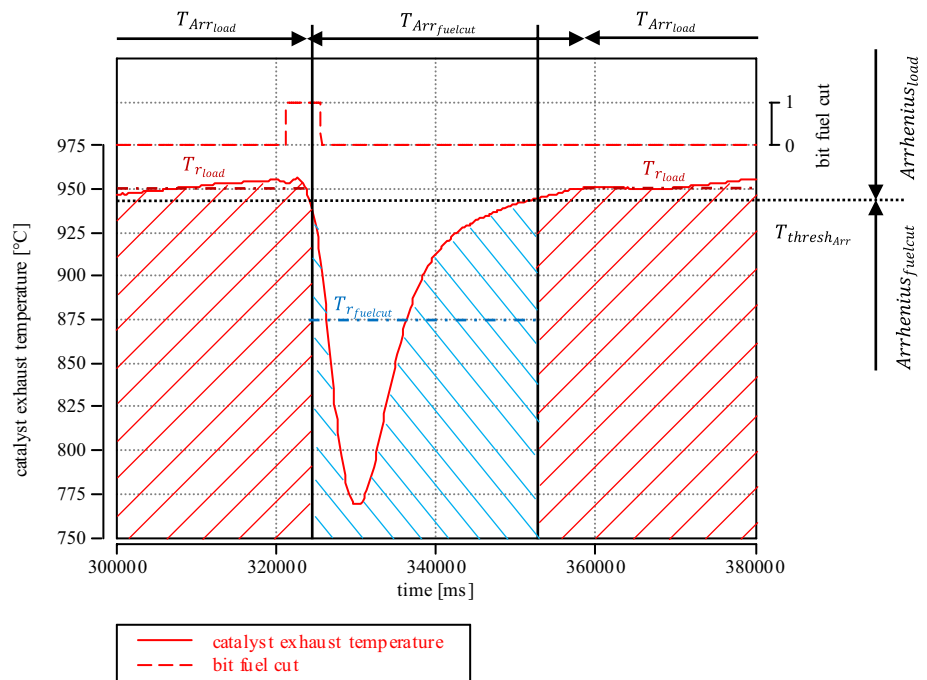**Fig. 14** Separation of Arrhenius equation in "load" and "fuel cut" as an example of #B

Table 3 Synthetic aging duration of exhaust systems with different fuel-cut frequencies, as well as their factorization $F_{\text{Arr}_{\text{heatloss}}}$

Exhaust system ID	FC interval (s)	FC duration (s)	Aging duration (h)	$T_{r_{\text{load}}}$	$S_{\text{Arr}_{\text{load}}}$	$T_{r_{\text{fuelcut}}}$	$S_{\text{Arr}_{\text{fuelcut}}}$	$S_{\text{Arrhenius}}$	Aging diff. (%)	$F_{\text{Arr}_{\text{heatloss}}}$
#A	Constant	–	50	943.6	49.32	949.2	1.31	50.63	100.0	+1.00
#C	120	3		948.2	31.32	920.1	20.63	51.95	102.6	+0.97
#D	60			949.3	27.35	908.6	28.49	52.84	104.4	+0.96
#E	30			950.5	10.88	902.5	44.06	54.94	108.5	+0.92

Fig. 15 Temperature histogram of the catalyst aging processes from top to bottom: #B, #C, #D, #E—including separation by $T_{\text{thresh}_{\text{Arr}}}$ into $T_{\text{r}_{\text{fuelcut}}}$ and $T_{\text{r}_{\text{load}}}$
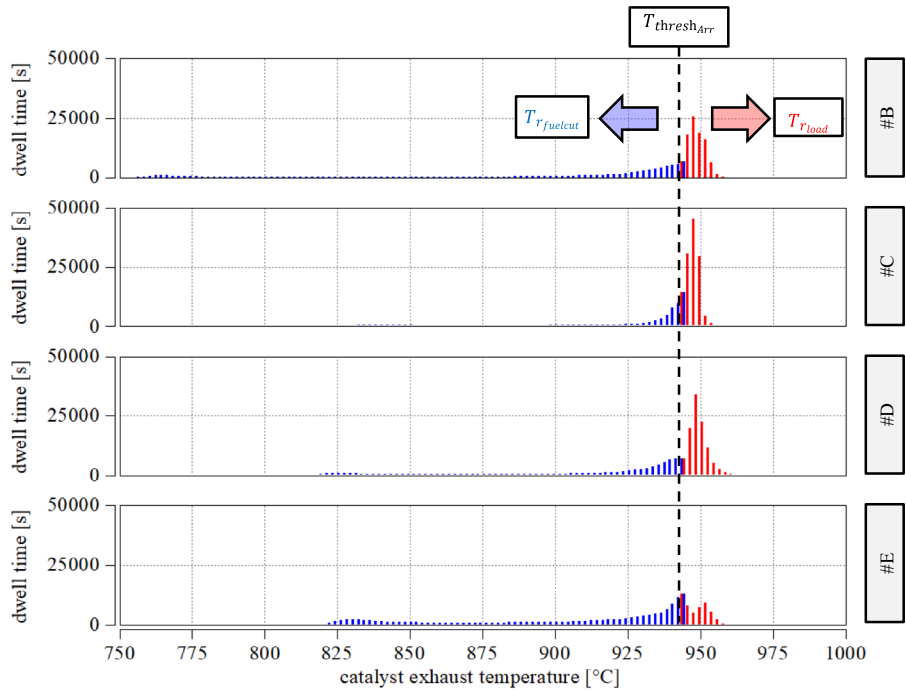
$$T_{\text{thresh}_{\text{Arr}}} = 0.995 * T_{\text{control}} = 0.995 * 950\,°\text{C} = 945\,°\text{C}$$

$$\text{Threshold for Arrhenius separation} \tag{15}$$

$T_{\text{r}_{\text{load}}}$ for temperatures $> 945\,°\text{C}$

$T_{\text{r}_{\text{fuelcut}}}$ for temperatures $< 945\,°\text{C}$

$$S_{\text{Arrhenius}} = S_{\text{Arr}_{\text{load}}} + S_{\text{Arr}_{\text{fuelcut}}} \quad \text{Summation of overall aging time.} \tag{16}$$

Figure 14 illustrates the temperature profile during a fuel-cut event as an example of catalyst #B. $T_{\text{thresh}_{\text{Arr}}}$ with its value of 945 °C separating the Arrhenius approach into $T_{\text{r}_{\text{load}}}$ and $T_{\text{r}_{\text{fuelcut}}}$.

Figure 15 gives an overview of the temperature histogram and the dwell time for each specific temperature bin with a 2 K range of the four different 50 h aging processes, used for calculation of t_e for catalyst #B, #C, #C, and #E.

The overall synthetic aging duration as a summation of both Arrhenius equations for the exhaust systems with different fuel-cut frequencies is listed in Table 3. To estimate the loss of heat input due to fuel-cut events, each specific value
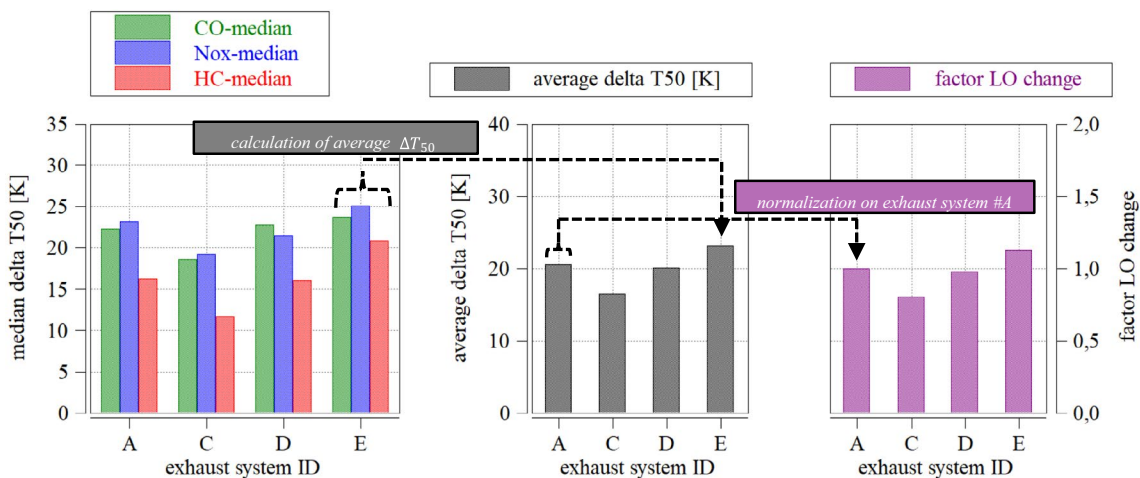

Fig. 16 Approach for conversion emission specific ΔT_{50} into LO factors

Table 4 Average ΔT_{50} based on aging processes and the aging process-specific $F_{LO_{change}}$

Exhaust system ID	FC interval (s)	FC duration (s)	Aging duration (h)	Average ΔT_{50} (K)	$F_{LO_{change}}$
#A	Constant	–	50	20.55	+ 1.00
#C	120	3		16.49	+ 0.80
#D	60			20.12	+ 0.98
#E	30			23.19	+ 1.13

Table 5 Calculation of an oxidation factor as an additional aging mechanism

Exhaust system ID	FC interval (s)	FC duration (s)	Aging duration (h)	$F_{Arr_{heatloss}}$	$F_{LO_{change}}$	F_{Oxi}
#A	Constant	–	50	+ 1.00	+ 1.00	± 0.00
#C	120	3		+ 0.97	+ 0.80	− 0.17
#D	60			+ 0.96	+ 0.98	+ 0.02
#E	30			+ 0.92	+ 1.13	+ 0.21

for $S_{Arrhenius}$ was normalized to exhaust system #A, the aging process without any fuel cut. With the help of this factor $F_{Arr_{heatloss}}$, the correlation between the increasing amount of fuel-cut events and the decrease of heat loss is obvious. The more fuel-cut events an aging process contains, the higher the heat losses and less profound thermal sintering processes occur. In practice, catalyst #E has to be aged 8.5% longer on the test bench to reach the same thermal sintering effect as catalyst #A.

4.3.3 T50 shift as a factor for reduction light-off capabilities

Prior explained delta heat maps permit an efficient overview regarding conversion ratio modification. However, they do not allow to directly identify the performance decrease as a characteristic number. To receive a practical value for the assessment of catalyst aging due to oxidation processes, the overall degradation of the exhaust system is described by use of the ΔT_{50} temperature. ΔT_{50} is defined by the median of all light-off curves set up with an exhaust mass flow between 100 and 400 kg/h for CO, HC, and NO_x. Catalyst aging is usually not emission species specific, which means that a degradation of the listed harmful gaseous occurs in comparable intensities at the same time. Therefore, the ΔT_{50} for CO, HC, and NO_x is averaged for each exhaust system (Fig. 16). The result is a value describing the degradation as a characteristic number for each catalyst, which allows a factorization, according to the chapter 4.3.3, normalized to catalyst exhaust system #A (Table 4). Comparing the ΔT_{50} for the individual systems with the reference system #A, stronger deviations of the catalyst performance are observed

than expected by calculation by the Arrhenius equation in Table 3.

4.3.4 Calculation of an oxidation aging factor

In chapter 4.3.2 and 4.3.3, characteristic numbers for $F_{Arr_{heatloss}}$ and $F_{LO_{change}}$ have been set up for each exhaust system describing the loss of catalytic efficiency due to aging procedures different fuel-cut frequency. Due to similar constant boundary conditions except the variation of fuel-cut events, the overall aging can be defined as the sum of oxidation and thermal sintering, shown via Eq. (16). A factor describing the aging effects of additional oxidative processes can be derived as the difference between calculated $F_{Arr_{heatloss}}$ and measured $F_{LO_{change}}$. The results are illustrated in Table 5

$$F_{Oxi} = F_{LO_{change}} - F_{Arr_{heatloss}} \qquad \text{Oxidation factor.} \qquad (17)$$

Reference exhaust system #A was aged continuously without fuel cut, so that no additional degradation by oxidation processes has to be considered. #C was aged with the lowest fuel-cut frequency, exhibiting higher thermal sintering but low amount of oxidation processes resulting in lower overall catalyst aging. F_{Oxi} increases with the number of fuel-cut, respectively, oxidation processes within an aging procedure. Doubling the amount of fuel-cut events increases the overall aging by 13% with oxidation taking over the main mechanism of reduction compensating decreasing thermal sintering effects (Fig. 17).

Figure 18 illustrates the overall aging as the $F_{LO_{change}}$ over the fuel-cut intervals including the variety of fuel-cut
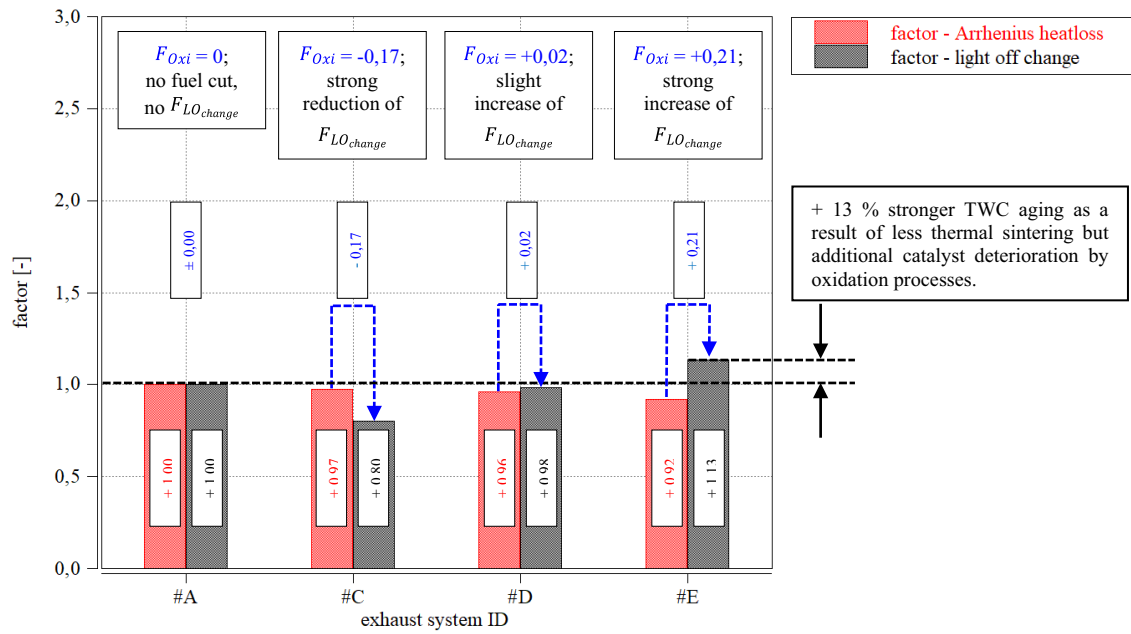
Fig. 17 Increased catalyst aging through fuel-cut event implementation
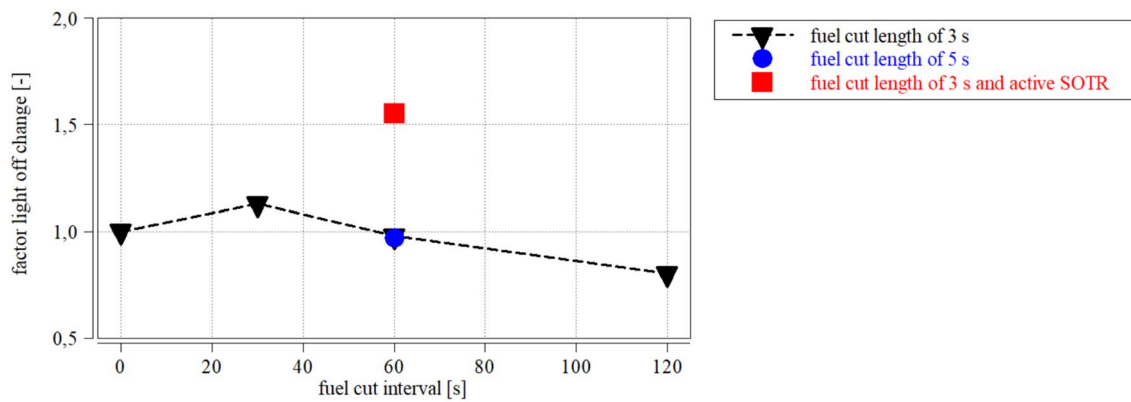

**Fig. 18** Change of light-off factor over fuel-cut interval

length and active SOTR function. Exhaust system #A without any fuel-cut interval and constant engine mode is listed over "0" fuel-cut interval, whereas exhaust system #D represents the initial point at 60 s for a comparison regarding the aging influence of fuel-cut length (#B) and active SOTR function (#F), calculated analog the procedure, explained before.

4.4 Thermal shock aging effects via SOTR function

4.4.1 Thermal shock characteristics with the modified engine test bench

High temperatures for sintering processes during catalyst aging can be obtained with presented engine bench setup via the exothermal reaction on the catalyst surface itself. Temperature upstream the catalyst shows a lower level compared to downstream measurements, as Fig. 6 already has already shown. The gas flow of the exhaust transports the thermal energy based of exothermic reactions downstream, so the overall temperature increases over substrate length.

Fig. 19 Comparison of temperature profiles during fuel-cut event with enabled (#F) and disabled (#D) SOTR function
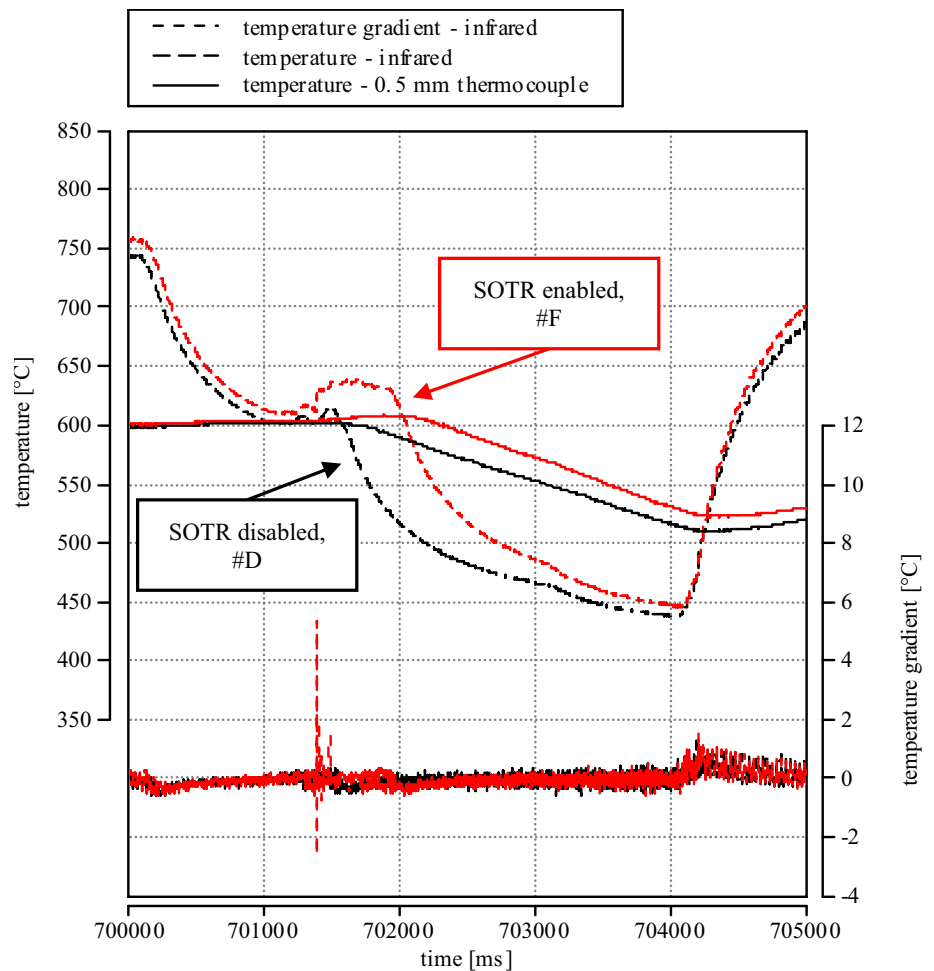
The optical thermography sensor faces on the middle of the catalyst's front face, measuring temperatures during active engine mode of about 750 °C. This level is higher than temperature measured upstream, but lower than temperatures measured downstream the catalyst (650 °C upstream, 950 °C downstream catalyst). Based on the geometry of the exhaust system, the optical sensor is facing the front face with an angle, lower than 180 °C. This is the reason why the sensor is also detecting thermic events on surfaces of the substrate channels, measuring additional exothermal reactions happening on the first TWC millimeters (Fig. 4—right side).

Figure 19 illustrates the difference between a fuel-cut event with and without an activated SOTR function (#F vs. #D). After inducing the fuel-cut event, in both catalysts, the temperatures, measured with the infrared sensor, decline due to introduction of fresh air. With some delay, both curves exhibit a temperature peak due to oxidation processes, which can be observed more intense with activated SOTR function. While overall temperature during a fuel-cut with an activated SOTR function lays within the acceptable boundary conditions, the first derivation

shows a drastic increase in temperature gradient compared to classic fuel cut. With an activated SOTR function, the increase shows values of up to 6 K/ms, whereas the values for a regular fuel cut do not increase measurably. Literature classifies values of about 6 K/ms as compatible for the substrate. During this study, these values have shown a distinct decrease of the overall performance of the exhaust system. To investigate the underlying effects, both substrates of #F and #D were analyzed via physisorption to determine a possible thermal mechanical damage.

These thermal effects were only measurable via the optical infrared sensor, as the inertia of 1.5 and even of 0.5 mm thermocouples did not resolve these fast temperature gradients. The damaging effect of the SOTR function seems to decrease slightly over the aging process of 50 h, possible due to declining exothermic reaction by to deactivation of the top layer PMG elements.

It is important to mention that the overall number of SOTR function used in this experiment during 50 h of aging at high exhaust temperatures added to more than 2.800, which would correspond to high mileage during normal driving. Sports cars for test track usually do not employ
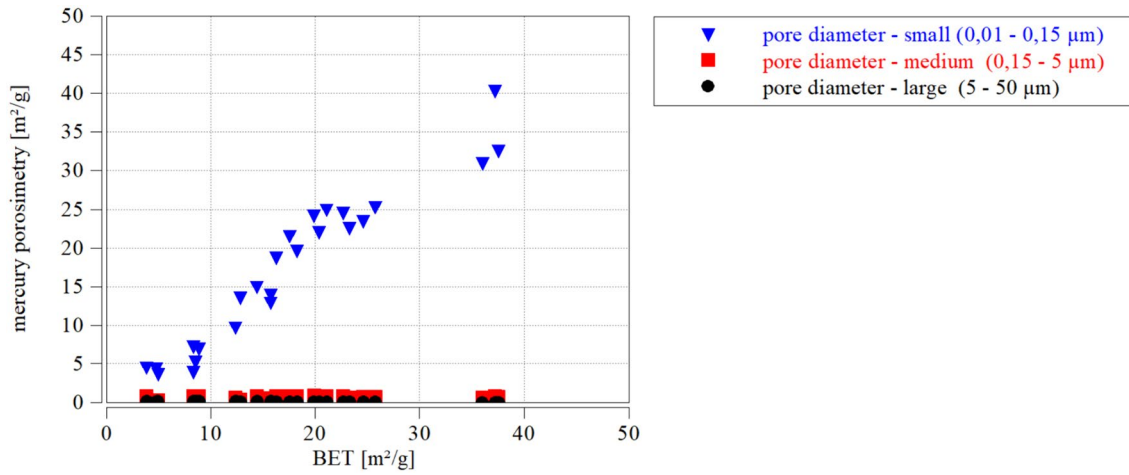
Fig. 20 Linear correlation of prior results of mercury intrusion polarography (QP) vs. BET results

Fig. 21 Abrasion due to thermal shock with thermal sintering on TWC upstream front face of catalyst #F (SOTR function)
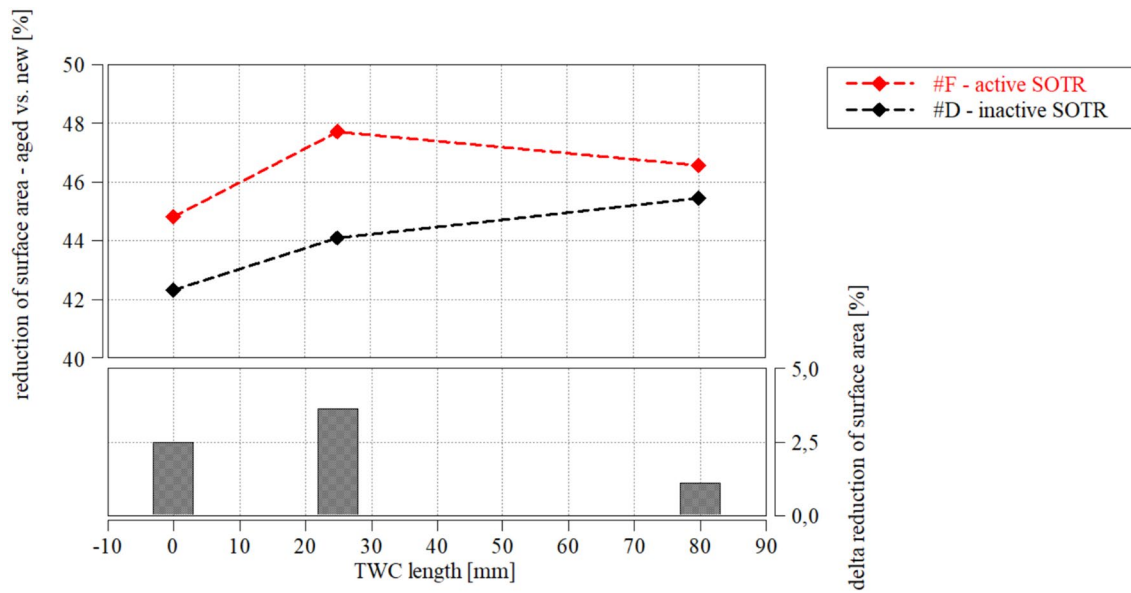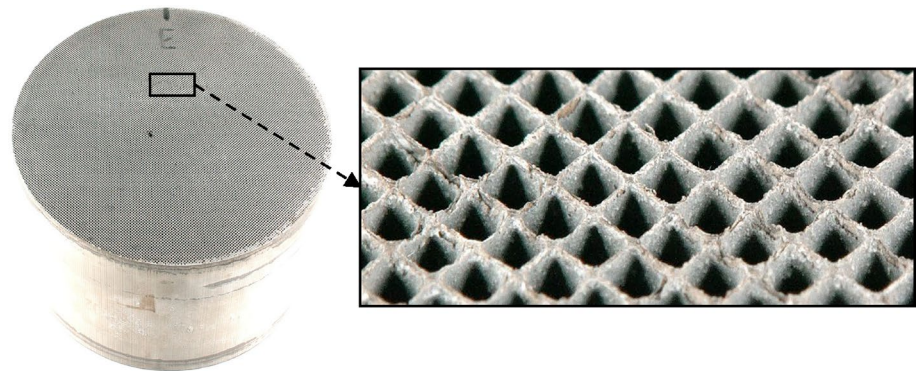

Fig. 22 Comparison of BET results of #F & #D with and w/o activated SOTR

exhaust aftertreatment systems, so that the effect is accepted and can be neglected. Engine calibration modifications can also reduce the effect, underlining the need to evaluate these parameters during development phases.

4.4.2 Physisorption via BET and mercury intrusion porosimetry

BET and mercury intrusion porosimetry (QP) were used to determine the overall decrease of the catalyst's surface due to thermal shock, induced via the SOTR function. With the help of the QP, different pore classifications have been defined using new and prior aged catalyst as kind of a best and worst case. The overall surface is dominated via small pore sizes (0.01–0.15 μm) for best (98%) and worst cases (93%), highly correlating with the results of the BET (Fig. 20). This is the reason why the BET is used during this study as a cost- and time-efficient method to determine the surface degradation of exhaust system #F and #D.

As explained before, the thermal shock occurs primarily on the front face of the TWC, damaging the surface (Fig. 21) and inducing a heat wave over the catalyst length. To determine the overall damage, the first catalyst of both exhaust systems have been extracted from the canning and the substrate was cut into disks with different sizes. Samples from front face upstream, front face downstream, as well as a disk at one-third of catalyst length have been removed with a thickness of 10 mm. For all three discs, small probes (10 × 10 mm) were prepared from the middle and analyzed via BET. The results given illustrated in Fig. 22: Comparison of BET results of #F & #D with and w/o activated SOTR as the reduction of surface in percent compared to a new catalyst of the same type.

The light-off results made via conversion heat maps can be confirmed by the BET results. Exhaust system #F shows a stronger aging with an active SOTR function via light-off, also expressed in a more profound surface degradation over the complete catalyst length. The measured thermal shock with a value of about 6 K/ms shows a stronger aging of the upstream volumes with a maximum degradation at 25 mm depth. In comparison to this, exhaust system #D has a surface reduction slightly increasing over the complete catalyst's length. Without an active SOTR function, exothermic reaction leads to an increasing temperature over the complete catalysts length, resulting in a stronger thermal sintering and so degradation. However, the SOTR function leads to a thermal shock, whose consequences overlap to the exothermic reactions. Its effect decreases over the catalyst length but rises the overall damaging level. The increasing peak at around one-third catalyst length is not unknown from field vehicles; similar effects have been observed on catalysts damaged by misfire.

5 Conclusion and outlook

The effect of fuel-cut events and their variation in terms of duration and frequency on catalyst aging was investigated on a turbo-charged eight-cylinder engine, which was modified by reducing the T3 temperature to guarantee the thermic durability of the turbocharger with the help of a secondary air system.

This study clearly demonstrated that catalyst aging is not driven by thermal sintering only. Oxidation processes induced by fuel-cut events are also partly responsible for a degradation regarding the catalyst conversion ratio as demonstrated via delta conversion heat maps. Therefore, the Arrhenius equation for a possible calculation of catalyst aging by time and maximum temperature is not able to predict all aging effects. This study has shown one approach to describe catalyst aging as a sum of different temperature levels for engine load and fuel-cut mode in combination with oxidizing deterioration processes. The higher the frequency of fuel-cut events, the higher the degradation due to oxidation, whereas thermal sintering processes are reduced. The strongest catalyst aging was observed by combined oxidation and thermal sintering, offering potentially a possible reduction of synthetic catalyst aging time by use of distinct fuel-cut events while generating the same degradation level.

The duration of a fuel cut might even demonstrate a positive effect on catalyst aging. The effect of cooling based on fresh air streaming through the substrate is higher than the effect of oxidation. The optimal duration of aging fuel-cut events during synthetic catalyst aging might be determined with the help of the oxygen sensors in the future. It might be feasible to stop the fuel-cut sequence after recognizing the signal change on the downstream sensor, so realistic oxidation processes on the complete catalyst surface with a minimum of heat loss are guaranteed.

The implementation of an active sound optimized torque reduction (SOTR) function on this engine bench setup has been investigated by the help of optical infrared sensor technology, measuring the temperature as well as temperature gradients on the catalyst front face. The secondary air injection, including its control path and mixer, enables high catalyst temperature, but functions as kind of a buffer, lowering the temperature gradients. Despite a slightly lower thermal sintering while having the same aging setup, the catalyst aged with an active SOTR function showed a stronger aging. The optical sensor recognized temperature gradients up to 6 K/ms, resulting in a

larger TWC surface degradation confirmed via BET. Signal comparisons have shown that effects generated by an SOTR function are only noticeable with the help of optical sensors. Even thermocouples with a diameter of 0.5 mm show a delay, which is too large for a possible recognition. These measurements prove that temperature gradients below 10 K/ms already have a negative impact on the thermal mechanic structure of a substrate and its washcoat.

An expansion of the aging duration for possible future studies is not recommended. An additional aging from 50 to 100 h did not show any differences regarding the overall quality of results.

Aside from the physisorption measurements already presented, chemisorption methods will be used for analyzing the surface activity as well as the sorption behavior in different areas within the monoliths. On top of that, a transmission electron microscope will be used to analyze the difference of the molecular structure and volume of the Cerium $Ce(II)_2$ and $Ce(III)$ to determine the mechanical stress within the washcoat due to oxidation processes. Modern exhaust systems contain more than one monolith, so that future component analysis will also include downstream substrates as well. To increase the resolution of the light-off curves, a synthetic hot-gas test bench can be used to control the exhaust temperature and mass flow more precisely.

Author contributions René Eickenhorst wrote the whole manuscript text and prepared all figures. All authors, René Eickenhorst and Prof. Dr. sc. techn. Koch, reviewed the manuscript.

Declarations

Conflict of interest On behalf of all authors, the corresponding author states that there is no conflict of interest.

References

1. Europäischen Union (EU).: Zur Ergänzung der Verordnung (EG) Nr. 715/2007 des Europäischen Parlaments und des Rates über die Typgenehmigung von Kraftfahrzeugen hinsichtlich der Emissionen von leichten Personenkraftwagen und Nutzfahrzeugen (Euro 5 und Euro 6), EU Verordnung 2017/1151 (2017).

2. Giuliano, M., Ricchiardi, G., Damin, A., Sgroi, M., Nicol, G., Parussa, F.: Thermal aging effects in a commercial three-way catalyst: physical characterization of washcoat and active metal evolution. Int. J. Automot. Technol. (2019). https://doi.org/10.1007/s12239.020.0031.x

3. Riegel, J., Neumann, H., Wiedenmann, H.-M.: Exhaust Gas Sensors for Automotive Emission Control. Elsevier Solid State Ionics, New York (2002)

4. Chris, J.L.: Datenbasierte Zustandsüberwachung in Personenkraftwaren mit Anwendung an einem Drei-Wege-Katalysator. Springer, Berlin (2016)

5. Dirk, K.F.: Modellbasierte On-Board-Diagnoseverfahren für Drei-Wege-Katalysatoren, Instituts für Regelungs- und Steuerungssysteme, Karlsruher Institut für Technologie (2010)

6. Grigorios, C.K., Anastasios, M.S.: Catalytic automotive exhaust aftertreatment. Prog. Energy Combust. Sci. **23**, 1–39 (1997)

7. Gong, C., Huang, K., Deng, B., Liu, X.: Catalyst light-off behavior of a spark-ignition LPG (liquefied petroleum gas) engine during cold start. Elsevier, Energy, New York (2011)

8. Abdolmaleki, S., Najafi, G., Ghobadian, B., Zakeri, A., Nejat, M.: Comparison of aged and fresh automotive three-way catalyst in driving cycle. J. Engine Res. **57**(57), 75–83 (2020)

9. Christian Hagelücken, I.-C.T.: Autoabgaskatalysatoren, expert Verlag (2016)

10. Bodo, O.: Ein vereinfachtes Modell des Lambda-geregelten Dreiwegekatalysators zum Einsatz in Motor-Steuergeräten zur On-Board-Diagnose, Energie-, Verfahrens- und Biotechnik der Universität Stuttgart, Universität Stuttgart (2003)

11. Ulla, L.: Deactivation correlations of PD/RH three-way catalysts designed for EURO IV emission limits. Department of Process and Environmental Engineering, University of Oulu (2003)

12. Konrad, R.: Abgastechnik für Verbrennungsmotoren. Springer, Berlin (2015)

13. Anja, K.M.: Bestimmung von Edelmetallgehalten in Autokatalysatoren; Department für Allgemeine, Analytische und Physikalische Chemie. Montanuniversität Leoben (2012)

14. Peter, C.F., Sieghard, E.W., Peter, S.T.: The limitation of the transmission electron microscope for characterization of supported metal catalysts. J. Catal. **33**, 233–248 (1973)

15. Brisley, R.J., O'Sullivan, R.D., Wilkins, A.J.J.: The effect of high temperature ageing on platinum-rhodium and palladium-rhodium three way catalysts. In: International Congress & Exposition. SAE Technical Paper 910175 (1991)

16. Ernst, W., Alois, H., Harald, P., Michael, T., Manuel, B.: Powertrain Calibration Techniques, SAE International (SAE 2019-24-0196) (2019)

17. Winkelhöfer, E., Hirsch, A., Hollerer, P.: Analysis of risk situations for TWC breakdown in normal engine and vehicle tests. In: 13th International Symposium on Propulsion Diagnostics, Baden-Baden, Germany (2018)

18. Winklhofer, E., Hirsch, A., Philipp, H., Trifterer, M., et al.: Powertrain calibration techniques. SAE Technical Paper 2019-24-0196 (2019)

19. Anna, F., Mats, L., Bengt, A.: Fuel-cut based rapid aging of commercial three way catalysts—influence of fuel-cut frequency, duration and temperature on catalyst activity. SAE International (SAE 2013–24–0156) (2013)

20. Maria, C.G., Giorgio, M.: Durability demonstration procedures of emission controll devices für Euro 6 vehicles, JRC Science and policy reports, Publications Office of the European Union (2014)

21. Eickenhorst, R.: An experimental study on aging effects of the air fuel ratio swing on modern gasoline three-way catalysts. Automot. Engine Technol. (2023). https://doi.org/10.1007/s41104-023-00132-0

22. Dipl.-Ing., R.H.: Genauigkeit und Reaktionszeiten von Temperaturmessgeräten, Bauphysik—Der Sachverständige, https://www.sv-huth.de/. Accessed 14 Nov 2023 (2011)

23. Sideris, M.: Methods for monitoring and diagnosing the efficiency of catalytic converters, Bd. 115. Studies in Surface Science and Catalysis. Elsevier (1998)

24. Taha, R., Duprez, D., Mouaddib-Moral, N., Gauthier, C.: Oxygen Storage Capacity of Three-way Catalysts: A Global Test for Catalyst Deactivation, Catalysis and Automotive Pollution Control IV. Elsevier Science B.V, New York (1998)

25. Cybulski, A., Moulijn, J.A.: Monoliths in heterogeneous catalysis. Catal. Rev. Sci. Eng. **36**, 179–270 (1994)

26. Please, C.P., Hagan, P.S., Schwendeman, D.W.: Light-off behaviour of catalytic converters. Soc. Ind. Appl. Math. **54**, 72–92 (1994)

27. Ignatov, D., Küpper, C., Pischinger, S., Bahn, M., Betton, W., Rütten, O., Weinowski, R.: Catalyst aging method for future emissions standard requirements, SAE International (2010)

28. EPA (Environmental Protection Agency).: Emission durability procedures and component durability procedures for new light-duty vehicles, light-duty trucks and heavy-duty vehicles; final rule and proposed rule, EPA—Federal Register/Vol. 71, No. 10, 40 CFR Part 86 (2006)

29. Lupescu, J.A.: Pd Model Catalysts: Effects of Aging Environment, Aging Duration and Interrupting Aging with Brief Air Pulses on Lean Pd Redispersion. University of Michigan (2016)